

Exoplanet population inference and the abundance of Earth analogs from noisy, incomplete catalogs

Daniel Foreman-Mackey^{1,2}, David W. Hogg^{2,3,4}, Timothy D. Morton⁵

ABSTRACT

No true extrasolar Earth analog is known. Hundreds of planets have been found around Sun-like stars that are either Earth-sized but on shorter periods, or else on year-long orbits but somewhat larger. Under strong assumptions, exoplanet catalogs have been used to make an extrapolated estimate of the rate at which Sun-like stars host Earth analogs. These studies are complicated by the fact that every catalog is censored by non-trivial selection effects and detection efficiencies, and every property (period, radius, *etc.*) is measured noisily. Here we present a general hierarchical probabilistic framework for making justified inferences about the population of exoplanets, taking into account survey completeness and, for the first time, *observational uncertainties*. We are able to make fewer assumptions about the distribution than previous studies; we only require that the occurrence rate density be a smooth function of period and radius (employing a Gaussian process). By applying our method to synthetic catalogs, we demonstrate that it produces more accurate estimates of the whole population than standard procedures based on weighting by inverse detection efficiency. We apply the method to an existing catalog of small planet candidates around G dwarf stars (Petigura *et al.* 2013). We confirm a previous result that the radius distribution changes slope near Earth’s radius. We find that the rate density of Earth analogs is about 0.02 (per star per natural logarithmic bin in period and radius) with large uncertainty. This number is much smaller than previous estimates made with the same data but stronger assumptions.

Subject headings: methods: data analysis — methods: statistical — catalogs — planetary systems — stars: statistics

¹To whom correspondence should be addressed: danfm@nyu.edu

²Center for Cosmology and Particle Physics, Department of Physics, New York University, 4 Washington Place, New York, NY, 10003, USA

³Max-Planck-Institut für Astronomie, Königstuhl 17, D-69117 Heidelberg, Germany

⁴Center for Data Science, New York University, 4 Washington Place, New York, NY, 10003, USA

⁵Department of Astrophysics, Princeton University, Princeton, NJ, 08544, USA

1. Introduction

NASA’s *Kepler* mission has enabled the discovery of thousands of exoplanet candidates (Batalha *et al.* 2013; Burke *et al.* 2014). While many of these candidates have not been confirmed as bona fide planets, there is evidence that the false positive rate is low (Morton & Johnson 2011; Fressin *et al.* 2013), enabling conclusions about the population of planets based on the catalog of candidates. Many of these planets orbit Sun-like stars (Petigura *et al.* 2013b), where the definition of Sun-like is given in terms of the star’s temperature and surface gravity. Given these catalogs, it is interesting to ask what we can say about the population of exoplanets as a function of their physical parameters (period, radius, *etc.*). Observational constraints on the population can inform theories of planet formation and place probabilistic bounds on the abundance of Earth analogs¹.

Petigura *et al.* (2013b) recently published an exoplanet population analysis based on an independent study of the *Kepler* light curves for 42,557 Sun-like stars. This study was especially novel because the authors developed their own planet search pipeline (*TERRA*; Petigura *et al.* 2013a) and determined the detection efficiency of their analysis empirically by injecting synthetic signals into real light curves measured by *Kepler*. The occurrence rate function determined by Petigura *et al.* (2013b) agrees qualitatively with previous studies of small planets orbiting Sun-like stars (Dong & Zhu 2013). In particular, both papers describe a “flattening” rate function (in logarithmic radius) for planets around Earth’s radius. Even though no Earth analogs were discovered in their search, Petigura *et al.* (2013b) used the small candidates that they did find to place an extrapolated constraint on the frequency of Earth-like exoplanets, assuming a flat occurrence rate density in logarithmic period.

A very important component of any study of exoplanet populations is the treatment of detection efficiency. Speaking qualitatively, in a transit survey, small planets with long periods are much harder to detect than large planets orbiting close to their star. This effect is degenerate with any inferences about the rate density and it can be hard to constrain quantitatively. In practice, there are three methods for taking this effect into account: (a) making conservative cuts on the candidates and assuming that the resulting catalog is complete (Catanzarite & Shao 2011; Traub 2012; Tremaine & Dong 2012), (b) asserting an analytic form for the detection efficiency as a function of approximate signal-to-noise (Youdin 2011; Howard *et al.* 2012; Dressing & Charbonneau 2013; Dong & Zhu 2013; Fressin *et al.* 2013; Morton & Swift 2013), and (c) determining the detection efficiency empirically by injecting synthetic signals into the raw data and testing recovery (Christiansen *et al.* 2013;

¹For our purposes, an “Earth analog” is an Earth-sized exoplanet orbiting a Sun-like star with a year-long period.

Petigura *et al.* 2013a,b).

There are two qualitatively different methods that are commonly used to infer the occurrence rate density from a catalog and a detection efficiency specification. The first is an intuitive method that we will refer to as “inverse-detection-efficiency” and the second is based on the likelihood function of the catalog given a parametric rate density. The inverse-detection-efficiency method involves making a histogram of the objects in the catalog where each point is weighted by its inverse detection probability. This method is very popular in the literature (Howard *et al.* 2012; Dong & Zhu 2013; Dressing & Charbonneau 2013; Swift *et al.* 2013; Petigura *et al.* 2013b) even though it is not motivated probabilistically. The alternative likelihood method models the catalog as a Poisson realization of the *observable* rate density of exoplanets taking the survey detection efficiencies and transit probabilities into account. This technique has been used to constrain parametric models—a broken power law, for example—for the occurrence rate density (Tabachnik & Tremaine 2002; Youdin 2011; Dong & Zhu 2013). As we show in Section 3, if we model the occurrence rate density as a piecewise constant function, the inverse-detection-efficiency method can be derived as a special case of the likelihood method with a specific set of assumptions.

In every previous study of exoplanet occurrence rates, the authors have assumed that the measurement uncertainties are negligible. This assumption is not justified because these uncertainties—especially on measurements (like exoplanet radius) that depend on the stellar parameters—can be large compared to the scales of interest. In this *Article*, we develop a flexible framework for probabilistic inference of exoplanet occurrence rate density that can be applied to incomplete catalogs with *non-negligible observational uncertainties*. Our method takes the form of a hierarchical probabilistic (Bayesian) inference. We generalize the method introduced by Hogg *et al.* (2010b) to account for survey detection efficiencies. We run tests on simulated datasets—comparing results with the standard techniques that neglect observational uncertainties—and apply our method to a real catalog of small planets transiting Sun-like stars (Petigura *et al.* 2013b).

For the purposes of this *Article*, we make some strong assumptions, although we argue that they are weaker than the implicit assumptions in previous studies. None of these assumptions is necessary for the validity of our general method but they do simplify the specific procedures we employ. We assume that

- the candidates in the catalog are independent draws from an inhomogeneous Poisson process set by the censored occurrence rate density,
- every candidate is a real exoplanet (there are no false positives),
- the observational uncertainties on the physical parameters are non-negligible but known

(the catalog provides probabilistic constraints on the parameters),

- the detection efficiency of the pipeline is known, and
- the $True^2$ occurrence rate density is *smooth*³.

The first assumption—conditional independence of the candidates—is reasonable since the dataset that we consider explicitly includes only single transiting systems (Petigura *et al.* 2013b). This is a limitation of the input catalog. When considering other datasets it will be interesting and important to take multiple transiting systems into account (Lissauer *et al.* 2011; Tremaine & Dong 2012; Fang & Margot 2012) and this would be possible using conditional distributions (as developed by Tremaine & Dong 2012). The second assumption—neglecting false positives—is also strong and only weakly justified by estimates of low false positive rates in the *Kepler* data (Fressin *et al.* 2013; Morton & Johnson 2011). For this *Article*, we will neglect this issue and only comment on the effects but the prior distributions published by Fressin *et al.* (2013) could be directly applied in a generalization of our method.

We must emphasize one very important consequence of our assumptions. We assume that the catalog of exoplanet candidates is only missing planets with probabilities given by the empirical detection efficiency. In detail this must be false; the detection efficiency we use doesn’t take into account the fact that the catalog doesn’t include multiple transiting systems. A large fraction of the transiting planets discovered by the *Kepler* transit search pipeline are members of multiple transiting systems (see Lissauer *et al.* 2011, for example). Since Petigura *et al.* (2013b) only detected at most one planet per system, their catalog is actually a list of planet candidates *without a more detectable companion*. The global effects of this selection are not trivial and an in-depth discussion is beyond the scope of this *Article* but all of the results should be interpreted with this caveat in mind.

Conditioned on our assumptions and the choices made in the planet detection, vetting and characterization pipeline (Petigura *et al.* 2013a,b), we constrain the rate density of small exoplanets orbiting Sun-like stars. As part of this analysis we also place probabilistic constraints on the rate density⁴ of Earth analogs Γ_{\oplus} , which we define as *the expected number of*

²In this *Article*, we use “*True*” to describe an observable (for example, the exoplanet occurrence rate density) that would be trivially measured in the limit of very high signal-to-noise data. We use “true” to describe a simulation quantity with a value exactly known to us.

³We give our definition of “smooth” in more detail below but our model is very flexible so this is not a strong restriction.

⁴In this *Article*, we use the word “rate” to indicate the dimensionless expectation value of a Poisson

planets per star per natural logarithmic bin in period and radius, evaluated at the period and radius of Earth

$$\Gamma_{\oplus} = \left. \frac{dN}{d \ln P d \ln R} \right|_{R=R_{\oplus}, P=P_{\oplus}}. \quad (1)$$

Since no Earth analogs have been detected, this constraint requires an extrapolation in both period and radius. [Petigura *et al.* \(2013b\)](#) performed this extrapolation by assuming that the period distribution of planets in a small bin in radius is flat, obtaining $\Gamma_{\oplus} \approx 0.12$. We relax this assumption and extrapolate only by assuming that the occurrence rate density is a smooth function of period and radius; we find lower values for Γ_{\oplus} . We enforce the smoothness constraint by applying a flexible Gaussian process regularization to the bin heights.

In the next Section, we introduce the concept of hierarchical inference, how it applies to the problem at hand, and we derive the importance sampling approximation to the marginalized likelihood (this is a generalization of the method from [Hogg *et al.* 2010b](#)). Then, in Section 3, we describe how to include detection efficiencies in this model and derive a probabilistic motivation for the standard inverse-detection-efficiency weighting procedure. We test our method on synthetic catalogs in Sections 5 and 6. In Section 7, we use the catalog of planet candidates and the empirically determined detection efficiency from [Petigura *et al.* \(2013b\)](#) to measure the occurrence rate density of Earth analogs.

2. A brief introduction to hierarchical inference

In this *Article*, we are asking the question: *what constraints can we put on the occurrence rate density of exoplanets given all the light curves measured by Kepler?* Throughout this *Article*, we use the notation $\Gamma_{\boldsymbol{\theta}}(\boldsymbol{w})$ for the occurrence rate density Γ —parameterized by the parameters $\boldsymbol{\theta}$ —as a function of the physical parameters \boldsymbol{w} (orbital period, planetary radius, *etc.*). In this framework, the occurrence rate density can be “parametric”—for example, a power law—or a “non-parametric” function—such as a histogram where the bin heights are the parameters $\boldsymbol{\theta}$. The light curve for a particular target k is \boldsymbol{x}_k and the *True* set of physical parameters for that same object is given by \boldsymbol{w}_k . A catalog provides a set of constraints on the parameters $\{\boldsymbol{w}_k\}$ conditioned on the set light curves $\{\boldsymbol{x}_k\}$.

Any inference about the rate density parameters can be formally addressed by evaluating

process and the words “rate density” to indicate a quantity that must be integrated over a finite bin in period and radius to deliver a rate.

the *marginalized likelihood function*

$$p(\{\mathbf{x}_k\} | \boldsymbol{\theta}) = \int p(\{\mathbf{x}_k\} | \{\mathbf{w}_k\}) p(\{\mathbf{w}_k\} | \boldsymbol{\theta}) d\{\mathbf{w}_k\} \quad (2)$$

where, as we mentioned above, $\{\mathbf{x}_k\}$ is the set of all light curves, one light curve \mathbf{x}_k per target k , $\boldsymbol{\theta}$ is the vector of parameters describing the population occurrence rate density $\Gamma_{\boldsymbol{\theta}}(\mathbf{w})$ and \mathbf{w}_k is the vector of physical parameters describing the planetary system (orbital periods, radius ratios, stellar radius, *etc.*) around target k . In this equation, our only assumption is that the datasets depend on the rate density of exoplanets only through the catalog $\{\mathbf{w}_k\}$. In our case, this assumption qualitatively means that the signals found in the light curves depend only on the actual properties of the planet and star, and not on the distributions from which they are drawn. It is worth emphasizing that—as we will discuss further below—the catalog only provides *probabilistic constraints* on $\{\mathbf{w}_k\}$; not perfect delta-function measurements.

In other words, we treat a catalog as being a dimensionality reduction of the raw data with all the relevant information retained. In the context of *Kepler*, the catalog reduces the set of downloaded pixel time series (approximately 70,000 data points for the typical *Kepler* target) to probabilistic constraints on a handful of physical parameters— \mathbf{w} from above—like the orbital period and planetary radius. If we take this set of parameters $\{\mathbf{w}_k\}$ as *sufficient statistics* of the data then we can, in theory, compute Equation (2)—up to an unimportant constant—without ever looking at the raw data again. This is permitted because the catalog provides constraints on the posterior probability of the parameters $\{\mathbf{w}_k\}$ under some choice of *interim prior*

$$p(\{\mathbf{w}_k\} | \{\mathbf{x}_k\}, \boldsymbol{\alpha}) = \frac{p(\{\mathbf{x}_k\} | \{\mathbf{w}_k\}) p(\{\mathbf{w}_k\} | \boldsymbol{\alpha})}{p(\{\mathbf{x}_k\} | \boldsymbol{\alpha})} . \quad (3)$$

The interim prior $p(\{\mathbf{w}_k\} | \boldsymbol{\alpha})$ is the prior function—parameterized by $\boldsymbol{\alpha}$ —that the author of the catalog chose when making their measurements.

It turns out that we can use these posterior measurements to simplify Equation (2) to a form that can, in many common cases, be evaluated efficiently. To find this result, multiply the integrand in Equation (2) by

$$\frac{p(\{\mathbf{w}_k\} | \{\mathbf{x}_k\}, \boldsymbol{\alpha})}{p(\{\mathbf{w}_k\} | \{\mathbf{x}_k\}, \boldsymbol{\alpha})} \quad (4)$$

and use Equation (3) to find

$$\frac{p(\{\mathbf{x}_k\} | \boldsymbol{\theta})}{p(\{\mathbf{x}_k\} | \boldsymbol{\alpha})} = \int \frac{p(\{\mathbf{w}_k\} | \boldsymbol{\theta})}{p(\{\mathbf{w}_k\} | \boldsymbol{\alpha})} p(\{\mathbf{w}_k\} | \{\mathbf{x}_k\}, \boldsymbol{\alpha}) d\{\mathbf{w}_k\} . \quad (5)$$

The data only enter this equation through the posterior constraints provided by the catalog $\{\mathbf{w}_k\}$! For our purposes, this is the *definition* of hierarchical inference.

The constraints in Equation (3) can always be—and often are—propagated as a list of N samples $\{\mathbf{w}_k\}^{(n)}$ from the posterior

$$\{\mathbf{w}_k\}^{(n)} \sim p(\{\mathbf{w}_k\} | \{\mathbf{x}_k\}, \boldsymbol{\alpha}) \quad . \quad (6)$$

We can use these samples and the Monte Carlo integral approximation to estimate the marginalized likelihood from Equation (5)—up to an irrelevant constant—as

$$p(\{\mathbf{x}_k\} | \boldsymbol{\theta}) \approx \frac{Z_{\boldsymbol{\alpha}}}{N} \sum_{n=1}^N \frac{p(\{\mathbf{w}_k\}^{(n)} | \boldsymbol{\theta})}{p(\{\mathbf{w}_k\}^{(n)} | \boldsymbol{\alpha})} \quad (7)$$

where the constant $Z_{\boldsymbol{\alpha}} = p(\{\mathbf{x}_k\} | \boldsymbol{\alpha})$ is not a function of the parameters $\boldsymbol{\theta}$. This is very efficient to compute as long as an evaluation of $p(\{\mathbf{w}_k\} | \boldsymbol{\theta})$ is not expensive. That being said, Equation (7) could be a high variance estimator of Equation (5), depending on the number of independent samples N and the initial choice of $p(\{\mathbf{w}_k\} | \boldsymbol{\alpha})$. Additionally, the support of $p(\{\mathbf{w}_k\} | \boldsymbol{\theta})$ in $\{\mathbf{w}_k\}$ space is restricted to be narrower than that of $p(\{\mathbf{w}_k\} | \boldsymbol{\alpha})$. Besides this caveat, in the limit of infinite samples, the approximation in Equation (7) becomes exact. Equation (7) is the *importance sampling approximation* to the integral in Equation (5) where the trial density is the posterior probability for the catalog measurements.

A very simple example is the familiar procedure of making a histogram. If you model the function $p(\{\mathbf{w}_k\} | \boldsymbol{\theta})$ as a piecewise constant rate density—where the step heights are the parameters—and if the uncertainties on the catalog are negligible compared to the bin widths then the maximum marginalized likelihood solution for $\boldsymbol{\theta}$ is a histogram of the catalog entries. The case of non-negligible uncertainties is described by [Hogg *et al.* \(2010b\)](#) using a method similar to the one discussed here.

3. Model generalities

In the inference procedure described above, we only discussed an abstract occurrence rate density. To make it more concrete, we'll model the catalog as a draw from the inhomogeneous Poisson process set by the *observable* rate density $\hat{\Gamma}_{\boldsymbol{\theta}}$. This leads to the previously known result (see [Tabachnik & Tremaine 2002](#); [Youdin 2011](#) for some of the examples from the exoplanet literature)

$$p(\{\mathbf{w}_k\} | \boldsymbol{\theta}) = \exp \left(- \int \hat{\Gamma}_{\boldsymbol{\theta}}(\mathbf{w}) d\mathbf{w} \right) \prod_{k=1}^K \hat{\Gamma}_{\boldsymbol{\theta}}(\mathbf{w}_k) \quad . \quad (8)$$

In this equation, the integral in the normalization term is the expected number of observable exoplanets in the sample.

The main thing to note here is that $\hat{\Gamma}_{\boldsymbol{\theta}}$ is the rate density of exoplanets that you would expect to observe taking into account the geometric transit probability and any other detection efficiencies. In practice, we can model the observable rate density as

$$\hat{\Gamma}_{\boldsymbol{\theta}}(\mathbf{w}) = Q_c(\mathbf{w}) \Gamma_{\boldsymbol{\theta}}(\mathbf{w}) \quad (9)$$

where $Q_c(\mathbf{w})$ is the detection efficiency (including transit probability) at \mathbf{w} and $\Gamma_{\boldsymbol{\theta}}(\mathbf{w})$ is the object that we want to infer: the *True* occurrence rate density. Up to this point, we haven’t discussed any specific functional form for $\Gamma_{\boldsymbol{\theta}}(\mathbf{w})$ and all of this derivation is equally applicable whether we model the rate density as, for example, a broken power law or a histogram.

The observed rate density $\hat{\Gamma}$ is a quantitative description of the rate density at which planets appear in the [Petigura *et al.* \(2013b\)](#) catalog; it is not a description of the *True* rate density of exoplanets. Inasmuch as the detection efficiency $Q_c(\mathbf{w})$ is calculated correctly, the function $\Gamma_{\boldsymbol{\theta}}(\mathbf{w})$ will represent the *True* rate density of exoplanets, at least where there is support in the data. In practice, an estimate of the detection efficiency will not include every decision or effect in the pipeline. One example in this case is that the completeness function does not account for the explicit removal of second (and third, and so on) planets. In principle a more complete description of the detection efficiency can be included and as this function becomes more accurate, our inferences about the *True* rate density $\Gamma_{\boldsymbol{\theta}}(\mathbf{w})$ will be less biased.

For the results in this *Article*, we will assume that the completeness function $Q_c(\mathbf{w})$ is known empirically on a grid in period and radius but that is not a requirement for the validity of this method. Instead, we could use a functional form for the completeness and even infer its parameters along with the parameters of the rate density.

Now, we can substitute Equation (8) into Equation (5) and apply the importance sampling approximation (Equation 7) to derive the following expression for the marginalized likelihood

$$\frac{p(\{\mathbf{x}_k\} | \boldsymbol{\theta})}{p(\{\mathbf{x}_k\} | \boldsymbol{\alpha})} \approx \exp \left(- \int \hat{\Gamma}_{\boldsymbol{\theta}}(\mathbf{w}) d\mathbf{w} \right) \prod_{k=1}^K \frac{1}{N_k} \sum_{n=1}^{N_k} \frac{\hat{\Gamma}_{\boldsymbol{\theta}}(\mathbf{w}_k^{(n)})}{p(\mathbf{w}_k^{(n)} | \boldsymbol{\alpha})} . \quad (10)$$

In this equation, we’re making the further assumption that the catalog treated the objects independently. This is a somewhat subtle point if we were to consider targets with more than one transiting planet—a point that we will return to below—but for the considerations

of the dataset considered in this *Article*, it is a justified simplification. In other words, we have per-object posterior samples

$$\mathbf{w}_k^{(n)} \sim p(\mathbf{w}_k | \mathbf{x}_k, \boldsymbol{\alpha}) \quad . \quad (11)$$

Equation (10) is the *money equation* for our method. It lets us efficiently compute the *marginalized likelihood of the entire set of light curves for a particular occurrence rate density*.

Inverse-detection-efficiency It’s now interesting to take a brief aside and discuss the connection between our model and the commonly used inverse-detection-efficiency procedure (Howard *et al.* 2012; Dressing & Charbonneau 2013; Petigura *et al.* 2013b). This procedure involves making a weighted histogram of the catalog entries where the weight for object \mathbf{w}_k is $1/Q_c(\mathbf{w}_k)$. This makes intuitive sense but the standard formulation does not have a clear probabilistic justification or interpretation.

If we model the occurrence rate density as a histogram with J fixed bin volumes Δ_j

$$\Gamma_{\boldsymbol{\theta}}(\mathbf{w}) = \begin{cases} \exp(\theta_1) & \mathbf{w} \in \Delta_1, \\ \exp(\theta_2) & \mathbf{w} \in \Delta_2, \\ \dots & \\ \exp(\theta_J) & \mathbf{w} \in \Delta_J, \\ 0 & \text{otherwise} \end{cases} \quad (12)$$

then Equation (8) becomes

$$\ln p(\{\mathbf{w}_k\} | \boldsymbol{\theta}) = \sum_{k=1}^K \sum_{j=1}^J \mathbf{1}[\mathbf{w}_k \in \Delta_j] [\ln Q_c(\mathbf{w}_k) + \theta_j] - \sum_{j=1}^J \exp(\theta_j) \int_{\Delta_j} Q_c(\mathbf{w}) d\mathbf{w} \quad (13)$$

where the indicator function $\mathbf{1}[\cdot]$ is one if \cdot is true and zero otherwise. If we take the gradient of this function with respect to $\boldsymbol{\theta}$ and set it equal to zero, we find the maximum likelihood result

$$\exp(\theta_j^*) = \frac{N_j}{\int_{\Delta_j} Q_c(\mathbf{w}) d\mathbf{w}} \quad (14)$$

where N_j is the number of objects that fall within the bin j . We estimate the uncertainty $\delta\theta_j$ on this value by examining the curvature of the log-likelihood function near the maximum and find

$$\frac{\delta \exp(\theta_j^*)}{\exp(\theta_j^*)} = \frac{1}{\sqrt{N_j}} \quad . \quad (15)$$

Since Equation (14) gives the maximum likelihood solution, this result is the minimum-variance estimator for the rate density when the completeness function $Q_c(\mathbf{w})$ is known and the catalog uncertainties are negligible. This is *almost* the same as the inverse-detection-efficiency procedure and if the completeness function is constant in each bin Δ , both methods give the same result. If the completeness function is not piecewise-constant on the same grid as the rate density inference, the inverse-detection-efficiency procedure will give a higher variance estimate of the occurrence rate density than Equation (14). In this *Article*, we don’t use either of these inverse-detection-efficiency procedures because they both fundamentally rely on the assumption of *negligible observational uncertainties*. By applying Equation (10), we derive the probabilistic generalization of this model in the next section but the result is no longer analytic.

Occurrence rate density parameterization & priors For the remainder of this *Article*, we also model the rate density as a two-dimensional histogram with fixed logarithmic bins in period and radius. When we include observational uncertainties—using Equation (10)—the maximum likelihood result is no longer analytic; Equation (14) is no longer applicable when the uncertainties are non-negligible. Therefore, if we want to compute the “best-fit” rate density, we can use a standard non-linear optimization algorithm. In the regions of parameter space that we tend to care about, the completeness is low and there are only a few observations with large uncertainties. In this case, we’re especially interested in probabilistic constraints on the occurrence rate density; not just the best-fit model. To do this, we must apply a prior $p(\boldsymbol{\theta})$ on the rate density parameters and generate samples from the posterior probability

$$p(\boldsymbol{\theta} | \{\mathbf{x}_k\}) \propto p(\boldsymbol{\theta}) p(\{\mathbf{x}_k\} | \boldsymbol{\theta}) \quad (16)$$

using Markov chain Monte Carlo (MCMC).

There is a lot of flexibility in the choice of functional form of $p(\boldsymbol{\theta})$. In the well-sampled parts of parameter space there are a lot of detected planets and the choice of prior makes little difference, but in the regions that we care about, the detection efficiency is low and applying a prior that captures our beliefs about the rate density is necessary. This will be especially important when we extrapolate the rate density function to the location of Earth—in Section 6—where no exoplanets have been found. Therefore, instead of using an uninformative prior, we want to use a prior that encourages the occurrence rate density to be “smooth” but it should be flexible enough to capture structure that is supported by the data. To achieve this, we model the logarithmic step heights as being drawn from a Gaussian process (Rasmussen & Williams 2006; Gibson *et al.* 2012; Ambikasaran *et al.* 2014).

This model encodes our prior belief that, on the grid scale that we consider, the rate density should be smooth but it is otherwise very flexible about the form of the function.

Mathematically, the Gaussian process density is

$$\begin{aligned} p(\boldsymbol{\theta}) &= p(\boldsymbol{\theta} | \mu, \boldsymbol{\lambda}) \\ &= \mathcal{N}[\boldsymbol{\theta}; \mu \mathbf{1}, \mathbf{K}(\{\Delta_j\}, \boldsymbol{\lambda})] \end{aligned} \quad (17)$$

where $\mathcal{N}(\cdot; \mu \mathbf{1}, \mathbf{K})$ is a J -dimensional Gaussian⁵ with a constant mean μ and covariance matrix \mathbf{K} that depends on the bin centers $\{\Delta_j\}$ and a set of hyperparameters $\boldsymbol{\lambda} = (\lambda_0, \lambda_P, \lambda_R)$. The covariance function that we use is an anisotropic, axis-aligned exponential-squared kernel so elements of the matrix are

$$\mathbf{K}_{ij} = \lambda_0 \exp\left(-\frac{1}{2} [\Delta_i - \Delta_j]^T \boldsymbol{\Sigma}^{-1} [\Delta_i - \Delta_j]\right) \quad (18)$$

where $\boldsymbol{\Sigma}^{-1}$ is the diagonal matrix

$$\boldsymbol{\Sigma}^{-1} = \begin{pmatrix} 1/\lambda_P & 0 \\ 0 & 1/\lambda_R \end{pmatrix} . \quad (19)$$

The Gaussian process model for the step heights given in Equation (17) is very flexible but the results will depend on the values of the hyperparameters μ and $\boldsymbol{\lambda}$. Therefore, instead of fixing these parameters to specific values, we add another level to our hierarchical probabilistic model and marginalize over this choice. In other words, we apply priors—uniform in the logarithm—on μ and $\boldsymbol{\lambda}$, and sample from the joint posterior

$$p(\boldsymbol{\theta}, \mu, \boldsymbol{\lambda} | \{\mathbf{x}_k\}) \propto p(\mu, \boldsymbol{\lambda}) p(\boldsymbol{\theta} | \mu, \boldsymbol{\lambda}) p(\{\mathbf{x}_k\} | \boldsymbol{\theta}) . \quad (20)$$

Strictly speaking, in this model, $p(\boldsymbol{\theta} | \mu, \boldsymbol{\lambda})$ can’t really be called a “prior” anymore and the constraints on the step heights are no longer independent.

There is an efficient algorithm called elliptical slice sampling (ESS; Murray *et al.* 2010; Murray & Prescott Adams 2010) for sampling the step heights $\boldsymbol{\theta}$ from the density in Equation (20). In practice, for problems with this specific structure, ESS outperforms more traditional MCMC methods commonly employed in astrophysics (e.g., Foreman-Mackey *et al.* 2012). Our implementation is adapted from Jo Bovy’s BSD licensed ESS code⁶. To simultaneously marginalize over the hyperparameter choice, we use the Metropolis–Hastings update

⁵ J is the total number of bins.

⁶https://github.com/jobovy/bovy_mcmc/blob/master/bovy_mcmc/elliptical_slice.py

from Algorithm 1 in [Murray & Prescott Adams \(2010\)](#). We tune the Metropolis–Hastings proposal by hand until we get an acceptance fraction of $\sim 0.2 - 0.4$ for the hyperparameters.

For all the results below, we run a Markov chain with 10^6 steps for the heights and update the hyperparameters every 10 steps. We only keep the final 2×10^5 steps and discard the earlier samples as burn-in. By estimating the empirical integrated autocorrelation time of the chain ([Goodman & Weare 2010](#)), we find that the resulting chain has $\gtrsim 4000$ independent posterior samples. These samples provide an approximation to the marginalized probability distribution for θ .

4. Data and completeness function

Using an independent exoplanet search and characterization pipeline, [Petigura *et al.* \(2013b\)](#) published a catalog of 603 planet candidates orbiting stars in their “Sun-like” sample of *Kepler* targets. For each candidate, [Petigura *et al.* \(2013b\)](#) used Markov chain Monte Carlo to sample the posterior probability density for the radius ratio, transit duration, and impact parameter assuming uninformative uniform priors. They then incorporated the uncertainties in the stellar radius and published constraints on the physical radii of their candidates. Given this data reduction and since we don’t have access to the individual posterior constraints on radius ratio and stellar radius, we can’t directly compute the importance weights $p(\{\mathbf{w}_k\} | \alpha)$ needed for Equation (7). For the rest of this *Article*, we’ll make the simplifying assumption that these weights are constant in log-period and log-radius but the results don’t seem to be sensitive to this specific choice.

[Petigura *et al.* \(2013b\)](#) did not publish or share posterior samples of their measurements of the physical parameter (Equation 6). They did publish a list of periods, radii and radius uncertainties based on their analysis. Assuming that there is no measurement uncertainty on the period measurement and that the radius posterior is Gaussian in linear radius (with a standard deviation given by the published uncertainty), we draw 256 samples for \mathbf{w}_k and use these as an approximation to the posterior probability function.

A huge benefit of this dataset is that Erik Petigura and collaborators published a rigorous analysis of the empirical end-to-end completeness of their transit search pipeline. Instead of choosing a functional form for the detection efficiency of the pipeline as a function of the parameters of interest, [Petigura *et al.* \(2013b\)](#) injected synthetic signals of known period and radius into the raw aperture photometry and determined the empirical recovery after the full analysis.

We use all the injected samples from [Petigura *et al.* \(2013b\)](#) to compute the mean

(marginalized) detection efficiency in bins of $\ln P$ and $\ln R$. In each bin, this efficiency is simply the fraction of recovered injections. For the purposes of this *Article*, we neglect the counting uncertainties introduced by the finite number of samples used to estimate the completeness. The largest injected signal had a radius of $16 R_{\oplus}$ but, because of the measurement uncertainties on the radii, we need to model the distribution at larger radii. To do this, we approximate the survey completeness for $R > 16 R_{\oplus}$ as 1.

Given our domain knowledge of how detection efficiency depends on the physical parameters, the intuitive choice would be to measure the survey completeness in radius ratio or signal-to-noise instead of period and radius. It is also likely that a change of coordinates would yield a higher precision result. That being said, it is still correct to measure the completeness in period and radius, and there are a few practical reasons for our choice. The main argument is that since the radius uncertainties are dominated by uncertainties in the stellar parameters, it is not possible to use the published catalog (Petigura *et al.* 2013b) to compute constraints on radius ratios. In the future, this problem would be solved by publishing a representation of *the full posterior density function for each object in the catalog*. In this case, the most useful data product would be *posterior samples for each target’s radius ratio and stellar radius*.

The detection efficiency also depends on the geometric transit probability R_{\star}/a . Since we are modeling the distribution in the period–radius plane, we need to compute the transit probability marginalized over stellar radius and mass. This marginalized distribution scales only with the period of the orbit as $\propto P^{-2/3}$. In theory, this marginalization should be over the *True* distribution of these parameters in the selected stellar catalog but we’ll approximate it by the empirical distribution; a reasonable simplification given the size of the dataset. At a period of 10 days⁷, the median transit probability in the selected sample of stars is 5.061% so we model the transit probability⁸ as a function of period as

$$Q_t(P) = 0.05061 \left[\frac{P}{10 \text{ days}} \right]^{-2/3}. \quad (21)$$

This expression is clearly only valid for $P \gtrsim 1.4$ days but the dataset that we are using (Petigura *et al.* 2013b) explicitly only includes periods longer than five days so this is not a problem. We’re using the *median* transit probability (instead of the mean) because it is a more robust estimator in the presence of outliers but in our experiments, the results do not seem to be very sensitive to this choice.

⁷This period is chosen arbitrarily because the power law only needs to be normalized at one point.

⁸We are using the letter Q to indicate probabilities since we are already using P to mean period.

5. Validation using synthetic catalogs

In order to get a feeling for the constraints provided by our method and to explore any biases introduced by ignoring the observational uncertainties, we start by “observing” two synthetic catalogs from qualitatively different known occurrence rate density functions. For each of these simulations, we take the completeness function computed by [Petigura *et al.* \(2013b\)](#) as given. In general, Equation (8) can be sampled using a procedure called thinning ([Lewis & Shedler 1979](#)) but for our purposes, we’ll simply consider a piecewise constant rate density evaluated on a fine grid in log-period and log-radius. For this discrete function, the generative procedure is simple;

1. loop over each grid cell i ,
2. draw Poisson random integer $K_i \sim \text{Poisson}(\hat{\Gamma}_i)$ with the observable rate density in the cell, and
3. distribute K_i catalog entries in the cell randomly.

We then choose fractional observational uncertainties on the radii from the [Petigura *et al.* \(2013b\)](#) catalog and apply them to the true catalog as Gaussian noise.

We generate synthetic catalogs from two qualitatively different rate density functions. Both distributions are generated by a separable model

$$\Gamma_{\theta}(\ln P, \ln R) = \Gamma_{\theta}^{(P)}(\ln P) \Gamma_{\theta}^{(R)}(\ln R) \quad (22)$$

but fit using the full general model. The first catalog—*Catalog A*—is generated assuming a smooth occurrence surface where both distributions are broken power laws. The second—*Catalog B*—is designed to be exactly the distribution inferred by [Petigura *et al.* \(2013b\)](#) in the range that they considered and then smoothly extrapolated outside that range. The catalogs generated from these two models are shown in [Figure 1](#) and [Figure 2](#), respectively and the data are available online⁹.

For each catalog, we directly apply both the inverse-detection-efficiency procedure as implemented by [Petigura *et al.* 2013b](#)¹⁰ and our probabilistic method, marginalizing over the hyperparameters of the Gaussian process regularization. [Figure 1](#) and [Figure 2](#) show the results of this analysis in both cases. In particular, the side panels compare the marginalized

⁹<http://dx.doi.org/10.6084/m9.figshare.1051864>

¹⁰Our implementation reproduces their results when applied to the published catalog.

occurrence rate density in period and radius to the true functions that were used to generate the catalogs. Figure 1 shows that even if the *True* rate density is a smooth function, the density inferred by the inverse-detection-efficiency method can appear to have sharp features. In this first example—where the true distribution is well described by our Gaussian process model—the probabilistic inference of the occurrence rate density is both more precise and accurate.

In the second example, the true rate density includes a sharp feature chosen to reproduce the result published by Petigura *et al.* (2013b). In this case, Figure 2 shows that the probabilistic constraints on the rate density are less precise but more accurate than results using the inverse-detection-efficiency method. This effect is most apparent in the parts of parameter space where the detection efficiency is low—long period and small radius.

When applied to either simulated catalog, the inverse-detection-efficiency method gives a high-variance estimate of the true occurrence rate density. One effect of this variance is that the inferred distribution will appear to have more small-scale structure than the true underlying distribution.

6. Extrapolation to Earth

As well as inferring the occurrence distribution of exoplanets, this dataset can also be used to constrain the rate density of Earth analogs. Explicitly, we constrain the occurrence rate density of exoplanets orbiting “Sun-like” stars¹¹, evaluated at the location of Earth:

$$\Gamma_{\oplus} = \Gamma(\ln P_{\oplus}, \ln R_{\oplus}) \quad (23)$$

$$= \left. \frac{dN}{d \ln P d \ln R} \right|_{R=R_{\oplus}, P=P_{\oplus}}. \quad (24)$$

That is, Γ_{\oplus} is the rate density of exoplanets around a Sun-like star (expected number of planets per star per natural logarithm of period per natural logarithm of radius), evaluated at the period and radius of Earth.

In Equation (23), we define “Earth analog” in terms of measurable quantities with no mention of habitability or composition. This might seem unsatisfying but the composition of an exoplanet is notoriously difficult to measure even with large uncertainty and any definition of habitability is still extremely subjective. With this in mind, we stick to the observable definition for this *Article*.

¹¹In this *Article*, we adopt the Petigura *et al.* (2013b) sample of G-stars as our definition of “Sun-like”.

Since no Earth analogs have been found, any constraints on this density must be extrapolated from the existing observations. This is generally done by assuming a functional form for the occurrence rate density, constraining it using the observed candidates and extrapolating. All published extrapolations are based on rigid models of the occurrence rate density (for example, a power law) fit to the catalog and evaluated at the location of Earth (Catanzarite & Shao 2011; Traub 2012). Petigura *et al.* (2013b) used their catalog of planet candidates to constrain the rate of Earth analogs in a specific period–radius bin assuming an extremely rigid model: *flat in logarithmic period*. These results are all sensitive to the choice of extrapolation function and the specific definition of “Earth analog”.

We weaken the assumptions necessary for extrapolation by only assuming that the distribution is smooth using the Gaussian process regularization described in Section 3. Under this model, the occurrence rate density at periods and radii where no objects have been detected will be constrained—with large uncertainty—by the heights of nearby bins. Therefore, even though there are no candidates that qualify as Earth analogs, we simply fit our model of the occurrence rate density in a large enough region of parameter space (including Earth) and compute the posterior constraints on Γ_{\oplus} . This works because the Gaussian process regularization actually captures our prior beliefs about the shape of the rate density function. This model—and any other extrapolation—will, of course, break down if there is an unmeasured sharp feature in the occurrence rate density near the location of Earth and our method is the most conservative extrapolation technique published to date.

For comparison, we also implemented and applied the extrapolation technique applied by Petigura *et al.* (2013b). Their method assumes that, for small planets ($1 \leq R/R_{\oplus} < 2$) on long periods ($P > 50$ days), the occurrence rate density is a flat function of logarithmic period or, equivalently, the cumulative rate is linear. Petigura *et al.* (2013b) used the candidates in their catalog to estimate the slope of the empirical cumulative period distribution and used that function to extrapolate. Instead of defining Γ_{\oplus} differentially, as we did in Equation (23), Petigura *et al.* (2013b) constrained the integral of the rate density over a box in period and radius ($1 \leq R/R_{\oplus} < 2$ and $200 \leq P/\text{day} < 400$). Since their model implicitly assumes a constant rate density across the bin, the differential rate is just their number divided by the bin area. This rate density (rate divided by bin volume) is what is shown as a comparison to our results in the figures.

Figures 3 and 4 compare our results and the results of the Petigura *et al.* (2013b) extrapolation procedure when applied to the synthetic catalogs. Since these catalogs were simulated from a known population model, we know the true value of Γ_{\oplus} and it is indicated in the figures with a vertical gray line. In both cases, our method returns a less precise but more accurate result for the rate density and the error bars given by the functional ex-

trapolation are overly optimistic. One major effect that leads to this bias is that the period distribution is not flat. Restricting the result to only include uniform models is equivalent to applying an extremely informative prior that doesn’t have enough freedom to capture the complexity of the problem. As a result, the posterior constraints on Γ_{\oplus} are dominated by this prior choice and the resulting uncertainties are much smaller than they should be.

7. Results from real data

Having developed this probabilistic framework for exoplanet population inferences and demonstrating that it produces reasonable results when applied to simulated datasets, we now turn to real data. As described in Section 4, we will use the catalog of small exoplanet candidates orbiting Sun-like stars published by [Petigura *et al.* \(2013b\)](#). This is a great test case because those authors empirically measured the detection efficiency of their pipeline as a function of the parameters of interest.

We directly applied our method to the [Petigura *et al.* \(2013b\)](#) sample and generated MCMC samples from the posterior probability for the occurrence rate density step heights, marginalizing over the hyperparameters of the Gaussian process model. The resulting MCMC chain is available online¹².

Figure 5 shows posterior samples from the inferred occurrence rate density as a function of period and radius conditioned on the catalog. The marginalized distributions are qualitatively consistent with the occurrence rate density measured using the inverse-detection-efficiency method with larger uncertainties.

The period distribution integrated over various radius ranges is shown in Figure 6. In agreement with [Dong & Zhu \(2013\)](#), we find that the period distribution of large planets ($R > 8 R_{\oplus}$) is inconsistent with the distribution of smaller planets. The rate density of large planets appears to monotonically increase as a function of log period while the distribution for small planets seems to turn over at a relatively short period (around 50 days) and decrease for larger periods.

The equivalent results for the radius distribution are shown in Figures 7 and 8. Figure 7 shows the log-radius occurrence rate density integrated over various logarithmic bins in period. The distributions in each period bin are qualitatively consistent; the rate density is dominated by small planets (around two Earth radii) with potential “features” near $R \sim 3R_{\oplus}$ and $R \sim 10R_{\oplus}$. These features appear in every period bin. They were also detected—using

¹²<http://dx.doi.org/10.6084/m9.figshare.1051864>

a completely different dataset and technique—by [Dong & Zhu \(2013\)](#) and a similar result is visible in the occurrence rate determined by [Fressin *et al.* \(2013\)](#), their Figure 7) at low signal-to-noise. Figure 8 shows the same result but presented as a function of linear radius. In these coordinates, the rate density in a single bin is no longer uniform; instead, scales as inverse radius.

Our constraint on the rate density of Earth analogs (as defined in Section 6) is in tension—even though our result has large fractional uncertainty—with the result from [Petigura *et al.* \(2013b\)](#). This is shown in Figure 9 where we compare the marginalized posterior probability function for Γ_{\oplus} to the published value and uncertainty. Quantitatively, we find that the rate density of Earth analogs is

$$\Gamma_{\oplus} = 0.017^{+0.018}_{-0.009} \text{ nat}^{-2} \quad (25)$$

where the “nat^{−2}” indicates that this quantity is a rate density, per natural logarithmic period per natural logarithmic radius. Converted to these units, [Petigura *et al.* \(2013b\)](#) measured $0.119^{+0.035}_{-0.046} \text{ nat}^{-2}$ for the same quantity (indicated as the vertical lines in Figure 9). This rate density is *exactly* what Petigura’s extrapolation model predicts but, for comparison, we can also integrate our inferred rate density over their choice of “Earth-like” bin ($200 \leq P/\text{day} < 400$ and $1 \leq R/R_{\oplus} < 2$) to find a *rate* of Earth analogs. The published rate is $0.057^{+0.022}_{-0.017}$ ([Petigura *et al.* 2013b](#)) and our posterior constraint is

$$\int_{P=200 \text{ day}}^{400 \text{ day}} \int_{R=1 R_{\oplus}}^{2 R_{\oplus}} \Gamma_{\theta}(\ln P, \ln R) d[\ln R] d[\ln P] = 0.016^{+0.011}_{-0.007} \quad (26)$$

Our inferred rate density of Earth analogs (Equation 25) is not consistent with the previously published result even though we use *exactly the same dataset*. This inconsistency is due to the different assumptions made. In particular, for their analysis, [Petigura *et al.* \(2013b\)](#) asserted that the period distribution for small planets on long orbits is flat in logarithmic period. If we enforce the same constraint, we reproduce their result but when we relax this assumption, allowing the data to constrain the period distribution, we find evidence for a *decreasing* period distribution as a function of logarithmic period (see Figure 6).

8. Discussion

We have developed a hierarchical probabilistic framework for inferring the population of exoplanets based on noisy incomplete catalogs. This method incorporates systematic treatment of observational uncertainties and detection efficiency. One major benefit of this framework is that it provides the best possible probabilistic measurements of the population

under the assumptions listed in Section 1 and repeated below. After demonstrating the validity of our method on two qualitatively different synthetic exoplanet catalogs, we run our inference on a published catalog of small exoplanet candidates orbiting Sun-like stars (Petigura *et al.* 2013b) to determine the occurrence rate density these planets as a function of period and radius. We extrapolate this measurement to the location of Earth and constrain the rate density of Earth analogs with large error bars. In order to perform this extrapolation, we don’t assume a specific functional form for the rate density. Instead, we only assume that it is a smooth function of logarithmic period and radius.

The occurrence rate density function that we infer is qualitatively consistent with previously published results using different inference techniques (Dong & Zhu 2013; Fressin *et al.* 2013; Petigura *et al.* 2013b). In particular, we find (see Figure 7) previously recorded features in the radius distribution around $R \sim 3 R_{\oplus}$ and $R \sim 10 R_{\oplus}$, although not at high signal-to-noise. We find that the period distributions for planets in different radius bins are different, in qualitative agreement with previous results (Dong & Zhu 2013). Figure 6 shows that larger planets tend to be on longer periods than smaller planets.

In detail, any inference of the exoplanet population depends on the choices made in the pipeline that creates the catalog. Our results are based on a catalog that only includes single transiting systems (Petigura *et al.* 2013b) so our conclusions—and theirs—must be considered with this in mind. In particular, the exclusion of second (and third, and so on) planets must suppress the inferred rate density, especially at long periods and small radii.

Our extrapolation of the rate density to the location of Earth is more general and conservative than any previously published method. We find a rate density of Earth analogs that is inconsistent with the result published by Petigura *et al.* (2013b). This discrepancy can be largely attributed to the rigidity of the assumptions about the period distribution. Our extrapolation is also less confident than previous measurements. Again, this difference is due to the fact that we allow a much more flexible extrapolation function. This is another illustration that, against the standard data analysis folklore, the correct use of flexible models is *conservative*.

In contrast to previous work, we don’t define “Earth analog” in terms of habitability or composition. Instead, we advocate for a definition in terms of more directly observable quantities (in this case, period and radius). Furthermore, we define Γ_{\oplus} as a rate density (per star per logarithmic period per logarithmic radius) so that its value doesn’t depend on choices about the “Earth-like” bin.

In our analysis we make a few simplifying assumptions. Every assumption has an effect on the results and could be relaxed as an extension of this project. For completeness, we list

and discuss the effects of our assumptions below.

- **Conditional independence** We assume that every object in the catalog is a conditionally independent draw from the observable occurrence rate density. This is a bad assumption when applying this method to a different catalog where multiple transiting systems are included. In practice, the best first step towards relaxing this assumption is probably to follow Tremaine & Dong (2012) and assume that the mutual inclination distribution is the only source of conditional dependence between planets. For this *Article*, the assumption of conditional independence is justified because the dataset explicitly includes only systems with a single transiting exoplanet.
- **False positives** In our inferences, we assume that all of the candidates in the catalog are *True* exoplanets. The rate of false positives in the *Kepler* catalog has been shown to be low but not negligible (Morton & Johnson 2011; Fressin *et al.* 2013). Since some of the objects in the catalog are probably false positives, our inferences about the occurrence rate density are biased high but without explicitly including a model of false positives, it’s hard to say in detail what effect this would have on the distributions. In an extension of this work, we could incorporate the effects of false positives by switching to a mixture model (see Hogg *et al.* 2010a, for example) where each object is modeled as a mixture of *True* exoplanet and false positive. In this mixture model, the false positives would be represented using prior distributions similar to those used by Morton (2012) or Fressin *et al.* (2013).
- **Known observational uncertainties** To apply the importance sampling approximation to the published catalog, we assume that the measurement uncertainties are known and, in this case, Gaussian. The assumption of normally distributed uncertainties could be relaxed given a sampling representation of the posterior probability function for the physical parameters (period, radius, *etc.*). There is recent evidence that the stellar radii of *Kepler* targets might, on average, be underestimated (Bastien *et al.* 2014), introducing another source of noise. It is possible to relax the noise model and include effects like this but inference would be substantially more computationally expensive.
- **Given empirical detection efficiency** Petigura *et al.* (2013b) determined the end-to-end detection efficiency of their planet detection pipeline as a function of *True* period and radius by injecting synthetic signals into real light curves and testing recovery. We used these simulations as an exact representation of the detection efficiency of the catalog but there are several missing components. The biggest effect is probably the fact that this formulation doesn’t include the selection of only the *most detectable signal*

in each light curve. This bias will be largest in the parts of parameter space where the baseline detection efficiency is lowest: at long periods and small radius. As a result, our inferences (and the results from [Petigura *et al.* 2013b](#)) about the occurrence rate of small planets on long periods is probably *underestimated* relative to *Truth*. In detail there is another limitation due to the fact that the stellar parameters are only known noisily and the transit light curve only constrains the radius ratio. This means that the marginalized detection efficiency should be measured as a function of radius ratio and the interpretation in terms of *True* radius is only approximately correct. Given the size of the dataset and the number of injection simulations, this effect should be small.

- **Smooth rate function** Throughout our analysis, we make the prior assumption that the occurrence rate density is a smooth function of logarithmic period and radius. This model is useful because it allows us to make probabilistically justified inferences about the exoplanet population in regions of parameter space with low detection efficiency. The assumption that the rate density should be smooth is intuitive but there is no theoretical indication that it must be true at all scales. That being said, the Gaussian process regularization that we use to enforce smoothness is flexible enough to capture substantial departures from smooth if they were supported by the data.

Our assumptions are severe but we believe that this is the most conservative population inference method currently on the market.

Under the assumptions that we have made here, our inference of the occurrence rate density of exoplanets places a probabilistic constraint on the number of transiting Earth analogs in the existing *Kepler* dataset. If we adopt the definition of “Earth-like” from [Petigura *et al.* \(2013b\)](#), $200 \leq P/\text{day} < 400$ and $1 \leq R/R_{\oplus} < 2$), and integrate the product inferred rate density function and the geometric transit probability (Equation 21) over this bin, we find that the expected number of Earth-like exoplanets transiting the stars in the sample of Sun-like stars chosen by [Petigura *et al.* \(2013b\)](#) is

$$N_{\oplus, \text{transiting}} = 9.2^{+5.9}_{-4.0} \quad (27)$$

where the uncertainties are only on the expectation value and don’t include the Poisson sampling variance. This is an exciting result because it means that, if we can improve the sensitivity of exoplanet search pipelines to small planets orbiting on long periods, then we should find some Earth analogs in the existing data. Furthermore, because of the treatment of multiple transiting systems in the catalog, the *True* expected number of transiting Earth-like exoplanets orbiting Sun-like stars is probably larger than the values in Equation (27)!

Some of the caveats on the results in this paper are due to assumptions made for computational simplicity but a much more robust study would be possible given a complete representation of the posterior probability function for the physical parameters in the catalog. The use of MCMC to fit models to observations is becoming standard practice in astronomy and the results in many catalogs (including [Petigura *et al.* 2013b](#)) are given as statistics computed on posterior samplings. For the sake of hierarchical inferences like the method presented here, it would be very useful if the authors of upcoming catalogs also published samples from these distributions *along with the value of their prior function evaluated at each sample*. In this spirit, we have released the results of this paper as posterior samplings¹³ for the occurrence rate density function.

All of the code used in this project is available from <http://github.com/dfm/exopop> under the MIT open-source software license. This code (plus some dependencies) can be run to re-generate all of the figures and results in this *Article*; this version of the paper was generated with git commit `eeb90f6` (2014-06-11).

We would like to thank Erik Petigura (Berkeley) for freely sharing his data and code. It is a pleasure to thank Ruth Angus (Oxford), Tom Barclay (NASA Ames), Jo Bovy (IAS), Eric Ford (PSU), and Ben Montet (Caltech/Harvard) for helpful contributions to the ideas and code presented here. This project was partially supported by the NSF (grant AST-0908357), NASA (grant NNX08AJ48G), and the Moore–Sloan Data Science Environment at NYU. This research builds on ideas generated at a three-week workshop on “Modern Statistical and Computational Methods for Analysis of Kepler Data” at SAMSI in 2013 June. This research made use of the NASA *Astrophysics Data System*.

REFERENCES

- Adams, R. P., Murray, I., & MacKay, D. J. C. 2009, ICML, 2009, 9 ([online](#))
- Ambikasaran, S., Foreman-Mackey, D., Greengard, L., Hogg, D. W., & O’Neil, M. 2014, [arXiv:1403.6015](#)
- Bastien, F. A., Stassun, K. G., & Pepper, J. 2014, ApJ, 788, L9 ([arXiv:1405.0940](#))
- Batalha, N. M., Rowe, J. F., Bryson, S. T., *et al.* 2013, ApJS, 204, 24 ([arXiv:1202.5852](#))
- Brewer, B. J., & Stello, D. 2009, MNRAS, 395, 2226 ([arXiv:0902.3907](#))

¹³<http://dx.doi.org/10.6084/m9.figshare.1051864>

- Burke, C. J., Bryson, S. T., Mullally, F., *et al.* 2014, ApJS, 210, 19 ([arXiv:1312.5358](#))
- Carter, J. A., & Winn, J. N. 2009, ApJ, 704, 51 ([arXiv:0909.0747](#))
- Catanzarite, J., & Shao, M. 2011, ApJ, 738, 151 ([arXiv:1103.1443](#))
- Christiansen, J. L., Clarke, B. D., Burke, C. J., *et al.* 2013, ApJS, 207, 35 ([arXiv:1303.0255](#))
- Dong, S., & Zhu, Z. 2013, ApJ, 778, 53 ([arXiv:1212.4853](#))
- Dressing, C. D., & Charbonneau, D. 2013, ApJ, 767, 95 ([arXiv:1302.1647](#))
- Fang, J., & Margot, J.-L. 2012, ApJ, 761, 92 ([arXiv:1207.5250](#))
- Foreman-Mackey, D., Hogg, D. W., Lang, D., & Goodman, J. 2013, PASP, 125, 306 ([arXiv:1202.3665](#))
- Fressin, F., Torres, G., Charbonneau, D., *et al.* 2013, ApJ, 766, 81 ([arXiv:1301.0842](#))
- Gibson, N. P., Aigrain, S., Roberts, S., *et al.* 2012, MNRAS, 419, 2683 ([arXiv:1109.3251](#))
- Goodman, J. & Weare, J., 2010, Comm. App. Math. Comp. Sci., 5, 65
- Hogg, D. W., Angus, R., Barclay, T., *et al.* 2013, [arXiv:1309.0653](#)
- Hogg, D. W., Bovy, J., & Lang, D. 2010a, [arXiv:1008.4686](#)
- Hogg, D. W., Myers, A. D., & Bovy, J. 2010b, ApJ, 725, 2166 ([arXiv:1008.4146](#))
- Howard, A. W., Marcy, G. W., Bryson, S. T., *et al.* 2012, ApJS, 201, 15 ([arXiv:1103.2541](#))
- Lewis, P. A. W., & Shedler, G. S. 1979, Naval Research Logistics Quarterly, 26, 403
- Lissauer, J. J., Ragozzine, D., Fabrycky, D. C., *et al.* 2011, ApJS, 197, 8 ([arXiv:1102.0543](#))
- Morton, T. D. 2012, ApJ, 761, 6 ([arXiv:1206.1568](#))
- Morton, T. D., & Johnson, J. A. 2011, ApJ, 738, 170 ([arXiv:1101.5630](#))
- Morton, T. D., & Swift, J. J. 2013, [arXiv:1303.3013](#)
- Murray, I., Prescott Adams, R., & MacKay, D. J. C. 2010, JMLR: W&CP, 9, 541 ([arXiv:1001.0175](#))
- Murray, I., & Prescott Adams, R. 2010, Advances in Neural Information Processing Systems, 23, 1723 ([arXiv:1006.0868](#))

- Petigura, E. A., Marcy, G. W., & Howard, A. W. 2013a, *ApJ*, 770, 69 ([arXiv:1304.0460](#))
- Petigura, E. A., Howard, A. W., & Marcy, G. W. 2013b, *Proceedings of the National Academy of Science*, 110, 19273 ([arXiv:1311.6806](#))
- Rasmussen, C. E. & Williams, C. K. I. 2006 *Gaussian Processes for Machine Learning*, MIT Press ([online](#))
- Roberts, S., McQuillan, A., Reece, S., & Aigrain, S. 2013, *MNRAS*, 435, 3639 ([arXiv:1308.3644](#))
- Swift, J. J., Johnson, J. A., Morton, T. D., *et al.* 2013, *ApJ*, 764, 105 ([arXiv:1301.0023](#))
- Tabachnik, S., & Tremaine, S. 2002, *MNRAS*, 335, 151 ([arXiv:astro-ph/0107482](#))
- Traub, W. A. 2012, *ApJ*, 745, 20 ([arXiv:1109.4682](#))
- Tremaine, S., & Dong, S. 2012, *AJ*, 143, 94 ([arXiv:1106.5403](#))
- Youdin, A. N. 2011, *ApJ*, 742, 38 ([arXiv:1105.1782](#))

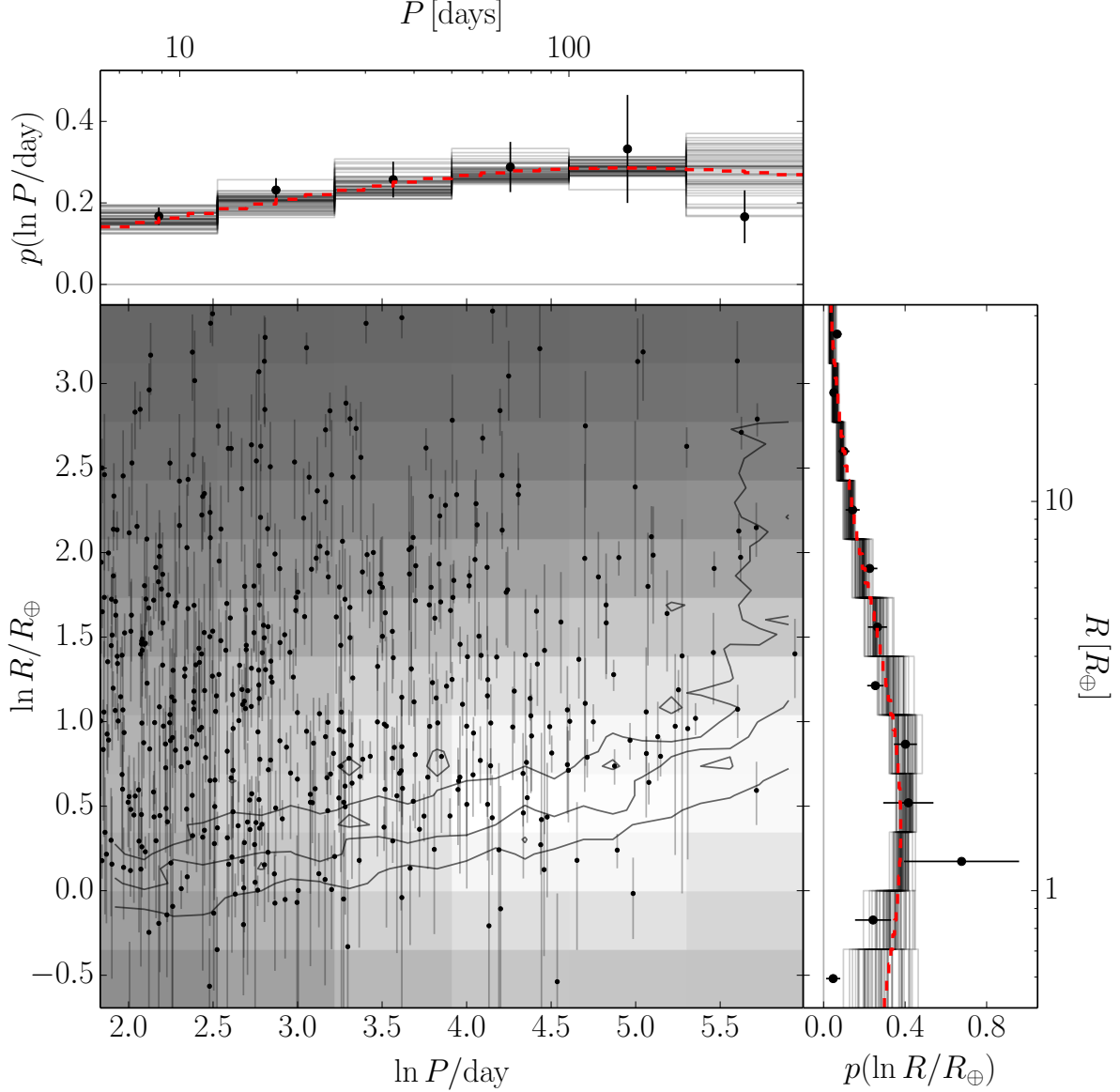


Fig. 1.— **Simulated data.** Inferences about the rate density based on the simulated catalog *Catalog A*. *Center:* the points with error bars show the exoplanet candidates in the simulated incomplete catalog, the contours show the survey completeness function (Petigura *et al.* 2013b), and the grayscale shows the median posterior occurrence surface. *Top and left:* the red dashed line shows the true distribution that was used to generate the catalog, the points with error bars show the results of the inverse-detection-efficiency procedure, and the histograms are posterior samples from the marginalized rate density as inferred by our method.

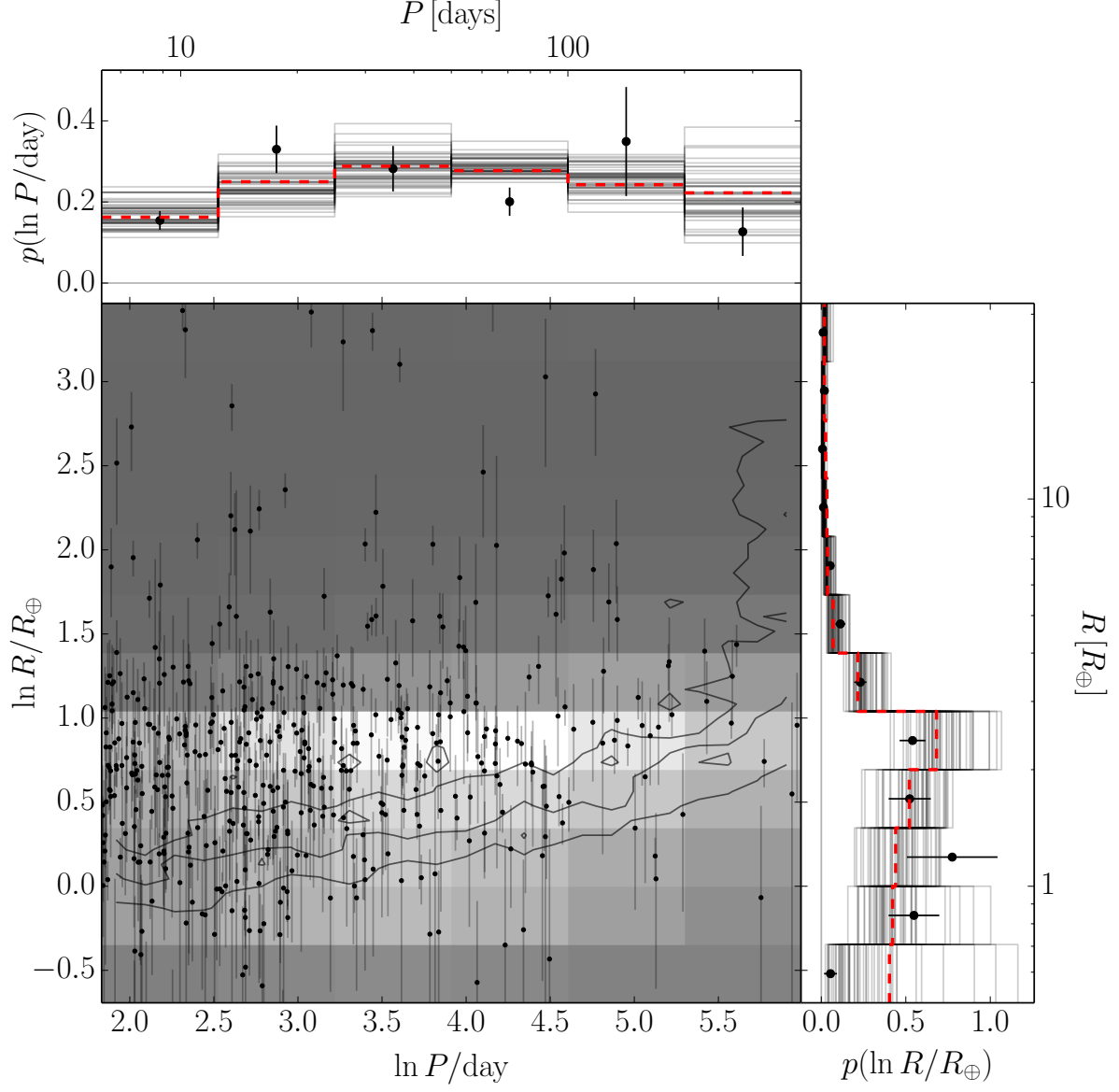


Fig. 2.— **Simulated data.** The same as Figure 1 for *Catalog B*.

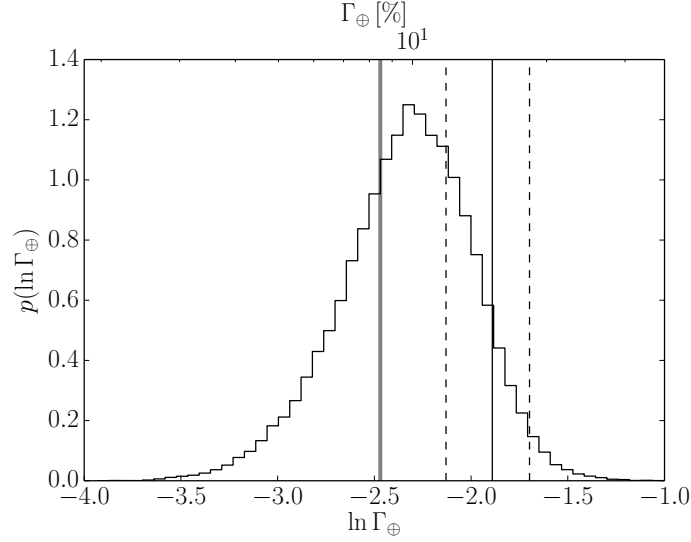


Fig. 3.— **Simulated data.** The extrapolated rate density of Earth analogs Γ_{\oplus} as inferred by the different techniques applied to the *Catalog A* simulation. Applying the method used by [Petigura *et al.* \(2013b\)](#) gives a constraint indicated by the vertical black line with error bars shown as dashed lines. The histogram is the MCMC estimate of our posterior constraint on this rate density and the true value is indicated as the thick gray vertical line.

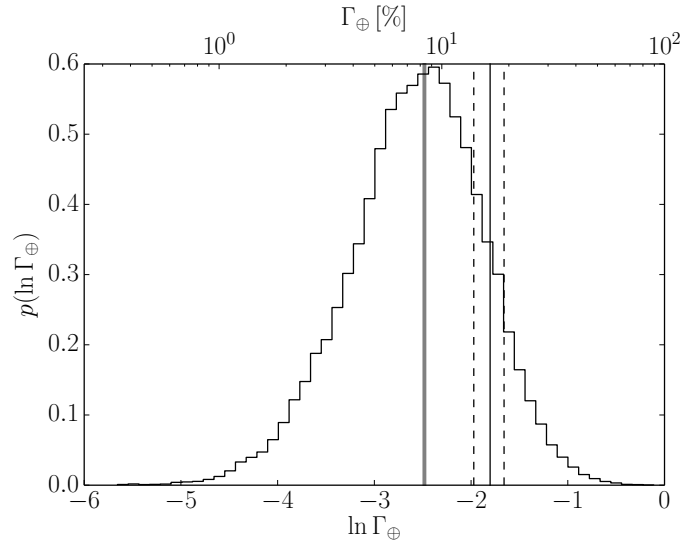


Fig. 4.— **Simulated data.** The same as Figure 3 for *Catalog B*.

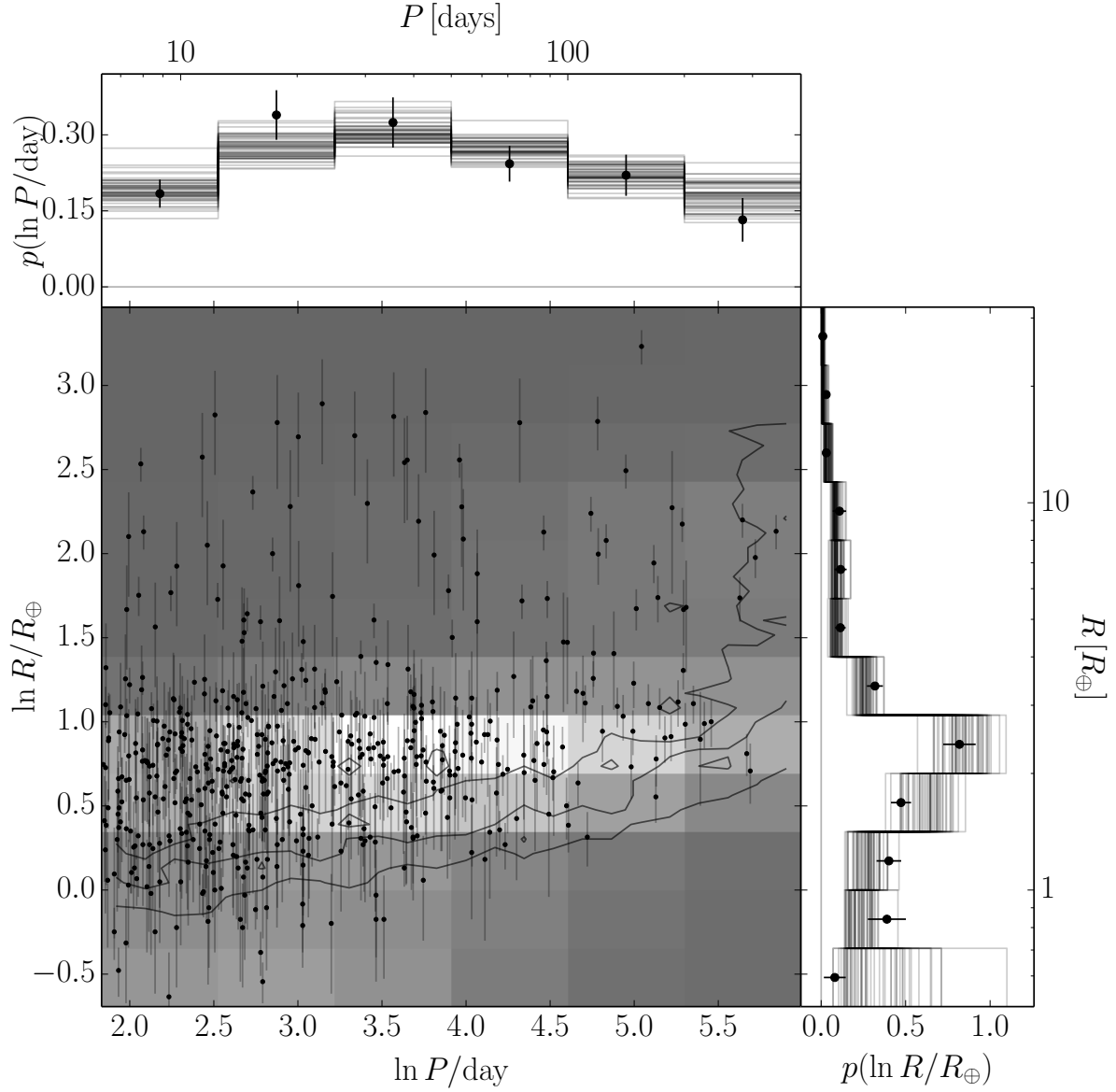


Fig. 5.— **Real data.** The same as Figure 1 when applied to the observed data from Petigura *et al.* (2013b). *Center:* the points with error bars show the catalog measurements, the contours show the survey completeness function, and the grayscale shows the median posterior occurrence surface. *Top and left:* the points with error bars show the results of the inverse-detection-efficiency procedure, and the histograms are posterior samples from the marginalized rate density as inferred by our method.

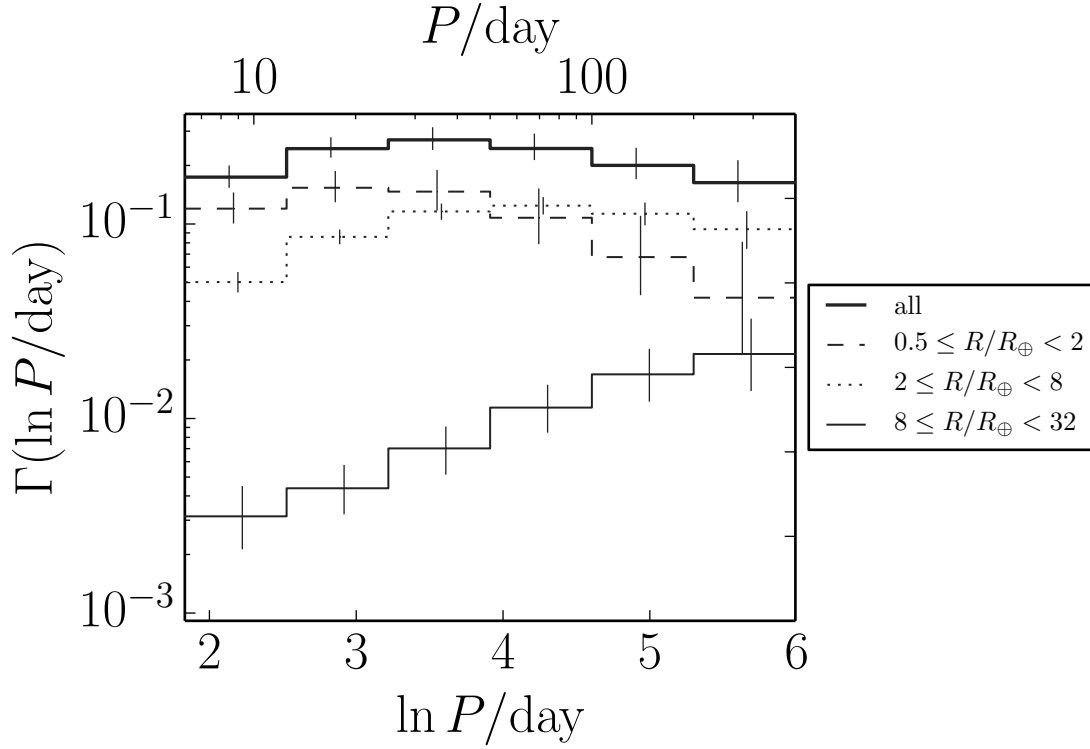


Fig. 6.— **Real data.** The occurrence rate density as a function of logarithmic period integrated over bins in logarithmic radius. The lines with error bars show the posterior sample median and 68th percentile and the line style specifies the radius bin. The period distribution for the largest planets in the sample ($8 \leq R/R_{\oplus} < 32$) continues to increase (as a function of $\ln P$) for all periods while the distribution seems to flatten and turn over at periods around 50 days.

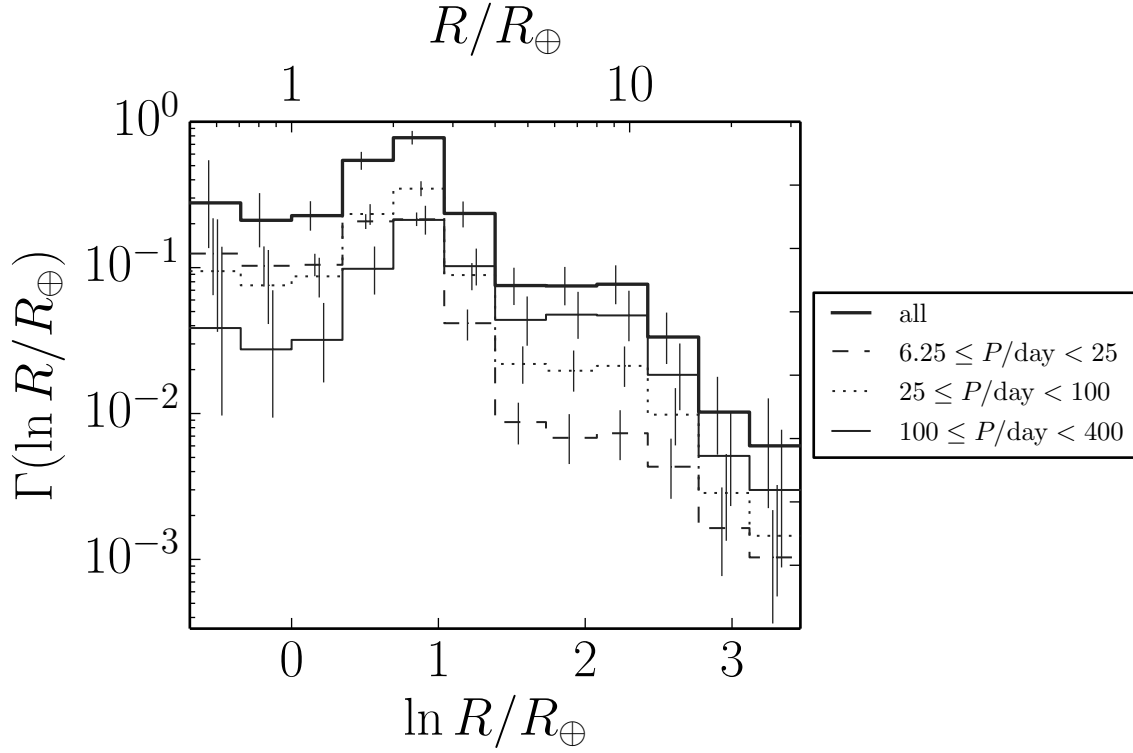


Fig. 7.— **Real data.** The occurrence rate density as a function of logarithmic radius integrated over bins in logarithmic period. The lines with error bars show the posterior sample median and 68th percentile and the line style specifies the period bin. The distributions in all the period bins are qualitatively consistent and there are plausibly features near $R \sim 3 R_{\oplus}$ and $R \sim 10 R_{\oplus}$.

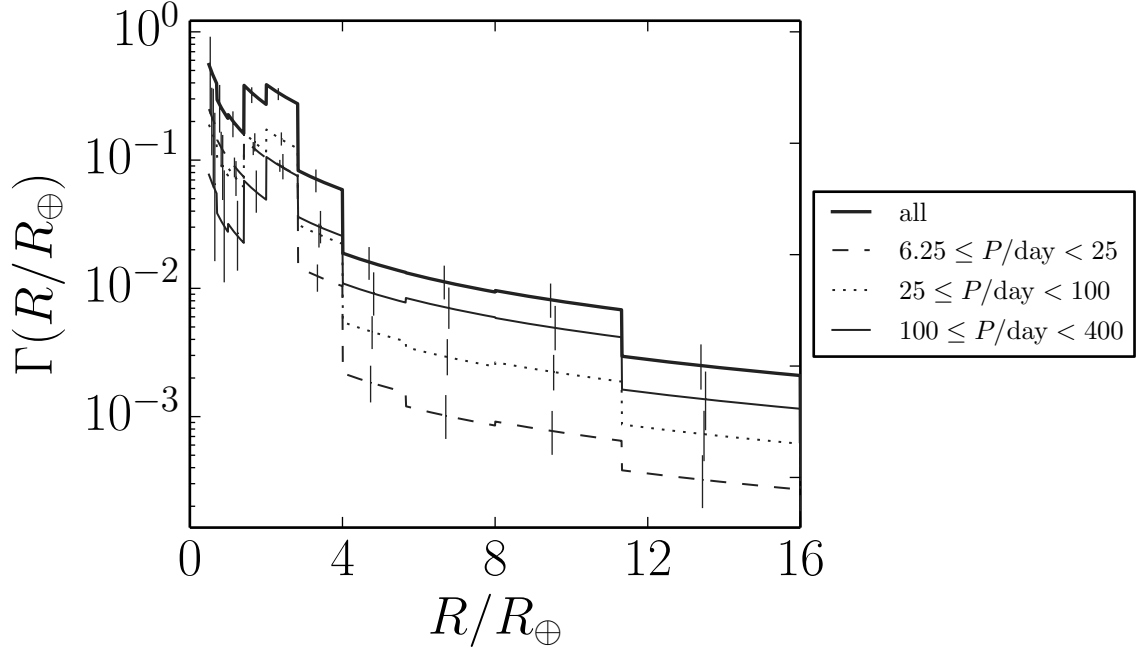


Fig. 8.— **Real data.** The same as Figure 7 but presented as a density in radius instead of logarithmic radius.

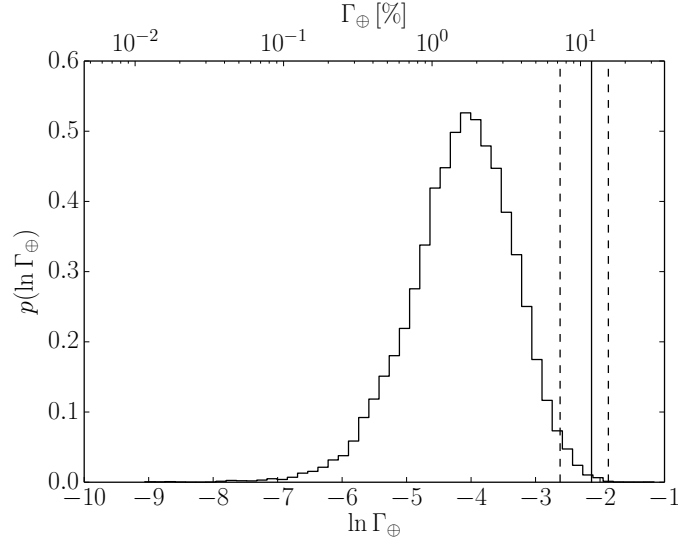


Fig. 9.— The extrapolated rate density of Earth analogs Γ_{\oplus} (the same as Figure 3 but applied to the catalog from [Petigura *et al.* 2013b](#)). The histogram is the MCMC estimate of our posterior constraint on this rate density. The vertical black line with error bars shown as dashed lines is the result from [Petigura *et al.* \(2013b\)](#) converted to a rate density by dividing by their bin volume.